

# Light Manipulation in Metallic Nanowire Networks with Functional Connectivity

Henning Galinski, Andrea Fratolocchi,\* Max Döbeli, and Federico Capasso\*

Subwavelength engineered materials, or metamaterials, designed to control the electromagnetic field are highly influenced by microelectronic circuit design, which manifests in the systematic assembly of well-defined and understood elements in periodic arrays.<sup>[1–11]</sup> In this communication, we explore a different approach, which takes inspiration from random network architectures. Complex networks arising in many different fields such as computer science (internet and the world wide web), biology (genes regulation, metabolic networks, food chains, neural networks), power transmission (large scale electric grids), social interactions (citation patterns) are all extremely robust and failure tolerant. In the internet<sup>[12]</sup> and other complex networks,<sup>[13]</sup> the removal of one or more nodes does not diminish the capability of the system to transmit and process information. Such robustness originates from the fact that the response of these systems is typically collective, driven by the functional connectivity among the network units. It is quite easy to understand that when the network size becomes sufficiently large, the overall system becomes extremely stable and robust.<sup>[14]</sup>

An intriguing question concerns the possibility of adopting these ideas as design principles for a new class of network metamaterials. At variance with classical metamaterials based on a geometric pattern design, a network metamaterial lacks unit cells and encompass randomly connected elements through a network of links. The response of the material (e.g., the reflectivity or transmissivity) depends on the interactions among the elements of the network, and is tailored by controlling its connectivity. In this design approach, the elements of the

network are not required to possess sophisticated electromagnetic behavior, because the response of the material is achieved through the interactions among the network units. Randomness has the advantage of being easily realized on large scales with minimal effort, and the interplay with light waves already reported a series of fascinating dynamics, ranging from energy harvesting, to lasing and beyond.<sup>[15–28]</sup> The main question is to find a process where the connectivity among disordered units can be tailored and controlled. We here use metallic nanowire networks fabricated by dealloying, a wet-chemistry technique.<sup>[29–37]</sup> These systems appear similar to porous materials, but with the unique difference that the short-range order, i.e., the network connectivity, can be here controlled in a deterministic fashion.

Dealloying is a reaction-diffusion process, first established by M. Raney in 1927.<sup>[38]</sup> This method is based on the selective dissolution of the less noble constituent of an alloy by the use of an acid or alkaline solution. The selective dissolution causes a reorganization of the remaining metal matrix, which is accompanied by the formation of a nanosized open network of pores.<sup>[29,35–37,39]</sup> The size of each pore is in the range of 5–30 nm, and is scalable via annealing or compositional changes.<sup>[30–34,40]</sup> Due to these features, dealloying is an ideal process to fabricate random nanowire networks from metallic thin films. Recent results showed that the dealloying of thin films is characterized by a linearly propagating diffusion front, which travels with a constant velocity of a few nanometers per second.<sup>[29]</sup> This effect furnishes a precise way to adjust the thickness of the dealloyed layer by controlling the dealloying/etching time. As we show below, dealloying for different times not only changes the thickness but also the connectivity of the nanowire network. Thus, dealloying allows to easily structure large areas in a fast and cost-effective fashion.

In our experiments, we deposited an initial 300 nm thick thin film of PtYAl on an amorphous Si<sub>3</sub>N<sub>4</sub>/Si substrate. The less noble Al in the Pt-alloy thin film is subsequently removed by immersing the coated substrates in a 4 M aqueous solution of NaOH. Networks with different connectivity are achieved by changing the etching time between 1 and 60 s. **Figure 1a** shows 2D reconstructions of dealloyed Pt<sub>55</sub>Y<sub>24</sub>Al<sub>21</sub> nanowire networks with different degrees of connectivity, based on focused ion beam (FIB) assisted scanning electron microscopy (SEM) images as discussed in the Supporting Information online text. The selective dissolution of the Al in the thin film caused the formation of a percolating open-porous nanostructure with 1500 connected nanowires per  $\mu\text{m}$  for a given cross-section in an open porous network. The nanowires have a mean branch length of  $50 \pm 10$  nm and a mean branch diameter  $\langle b \rangle$  of  $20 \pm 5$  nm. The mean pore intercept length of the porous network  $\langle L \rangle$ , i.e., the average distance between two metal/pore

H. Galinski, Prof. F. Capasso  
Harvard John A. Paulson School of Engineering  
and Applied Sciences  
Harvard University  
29 Oxford Street, Cambridge, MA 02138, USA  
E-mail: capasso@seas.harvard.edu



H. Galinski  
Laboratory for Nanometallurgy  
ETH Zurich  
Vladimir-Prelog-Weg 1-5/10, Zurich 8093, Switzerland  
Prof. A. Fratolocchi  
PRIMALIGHT  
Faculty of Electrical Engineering  
Applied Mathematics and Computational Science  
King Abdullah University of Science and Technology (KAUST)  
Thuwal 23955-6900, Saudi Arabia  
E-mail: andrea.fratolocchi@kaust.edu.sa  
M. Döbeli  
Ion Beam Physics  
ETH Zurich  
Otto-Stern-Weg 5, Zurich 8093, Switzerland

DOI: 10.1002/adom.201600580

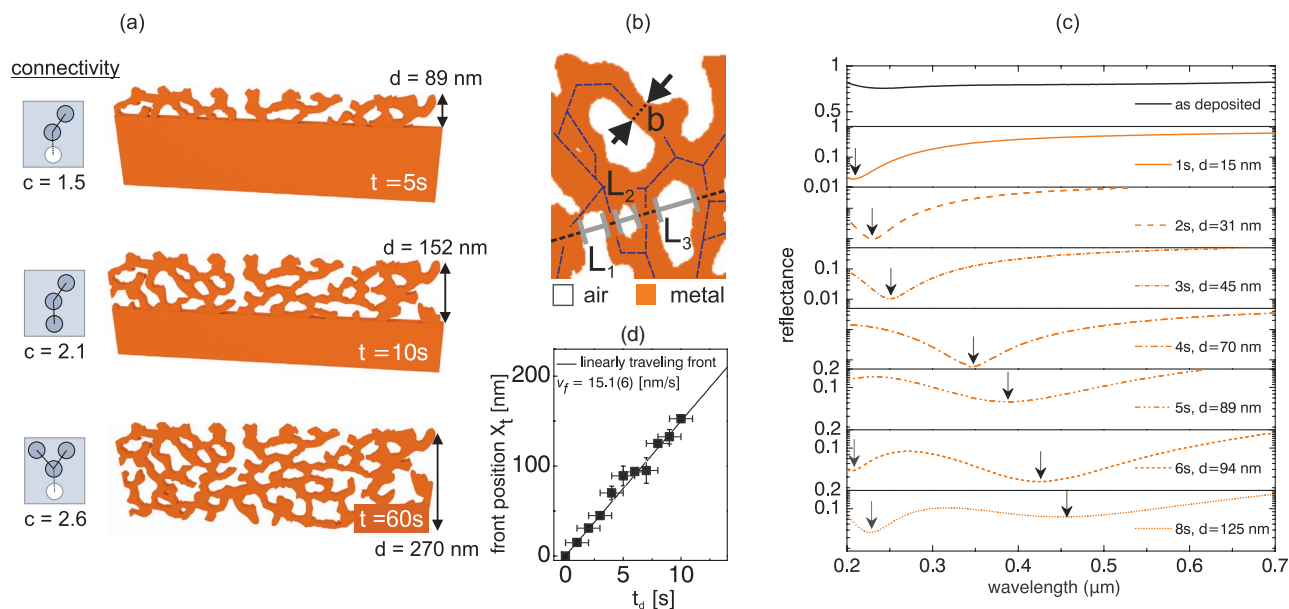


**Figure 1.** Nanostructure and controlled engineering of network metamaterials with different degrees of connectivity. a) Illustration of different degrees of connectivity  $c$  reached by dealloying Pt-Y-Al thin-films for different times  $t$ . The depicted network architectures are based on focused ion beam (FIB) assisted scanning electron microscopy images. b) Schematic cross-sectional view of a dealloyed nanostructure illustrating selected geometric parameters, such as the pore intercept length  $L$  and the branch diameter  $b$ . The mean branch diameter is  $20 \pm 5$  nm and the mean pore intercept length is  $35 \pm 5$  nm. The open porous network is formed by dissolving the less noble element (Al) in the alloy. c) Experimental near-normal incidence reflectance spectra as function of the dealloying time and thickness of the disordered layer, respectively. The minima of the reflectance spectra are indicated by black arrows. d) The position of the dissolution front is plotted as function of the etching time  $t_d$ . The dissolution front (grey arrow) travels with a constant speed of  $15 \pm 6$  nm s<sup>-1</sup>. The error bars in  $t_d$  reflect the uncertainties in measuring the etching time.

interfaces in a given direction (Figure 1b), is calculated to be  $35 \pm 5$  nm. As a result, the characteristic mean nanowire diameter and the mean pore intercept-length of the dealloyed thin film do not exceed  $0.2\lambda$  for the visible spectrum. It is to expect that the optical properties of this random network of subwavelength structures scale with the moments of the size distribution of its constituting elements, namely the nanowire length and mean branch diameter, the mean pore intercept length and their connectivity.

In order to determine the mean connectivity  $\langle c \rangle$ , defined as the average number of contacts of a nanowire per unit area, of the dealloyed thin films, FIB cross-section images of different dealloying states have been analyzed (see the Supporting Information online text for detailed information). The mean connectivity changes from  $\langle c \rangle \in [1.52, 2.59]$  with increasing thickness  $d \in [10\text{--}270\text{ nm}]$  of the dealloyed layer, as shown in Figure 1a. The change in connectivity can be interpreted as result of a continuous transition of the porous network, beginning with a channel-like 2D porosity with few interconnections at small etching times and ending with a fully percolating 3D porous network.

We employed Rutherford backscattering spectroscopy (RBS) to measure the thickness and composition of the dealloyed layer with high accuracy. RBS is an ideal technique for elemental depth profiling in thin films as it is nondestructive and highly quantitative.<sup>[29,41]</sup> In our study, RBS measurements are essential to quantify the controllability of the connectivity in the fabricated Pt-Y-Al thin film. Details on the RBS technique are found in the Supporting Information online text. The position of the dissolution front  $X(t)$  is calculated with respect to the initial

film thickness  $h_0$  and the thickness  $h(t_d)$  of the remaining dense Pt-Y-Al layer for a given etching time  $t_d$ , and reads  $X(t) = h_0 - h(t_d)$ . The velocity of the dissolution front  $X(t)$ , obtained by plotting the dissolution front position  $X(t)$  as function of the dealloying time  $t_d$  (see Figure 1d), is constant at  $15 \pm 6$  nm s<sup>-1</sup>. The thickness of the nanowire network including its connectivity can be therefore controlled with high precision, smaller than  $0.07\lambda$  for a wavelength  $\lambda > 200$  nm, assuming a minimal etching time of 1 s, which corresponds to a minimal increment of the dealloyed layer of 15 nm.

In order to measure the electromagnetic response of the samples, we measured the near-normal incidence reflectivity spectrum of an ensemble of samples, reporting the results of a set of samples dealloyed for different times in Figure 1c. A second set of reflectivity spectra is given in the Supporting Information online text, in conjunction with a data set with increased yttrium content, illustrating the effect of compositional changes as additional tuning parameter. By comparing the spectra obtained from samples with the same thickness  $d$ , we did not observe significant variations of the spectra, showing that the randomness of one sample is already averaging the electromagnetic response of the system. Figure 1c and the corresponding simulation in Figure 2a show a rich dynamical scenario as the dealloying time  $t_d$  is varied. The as-deposited dense Pt-Y-Al film behaves as a broadband reflector, as expected from a continuous metal film. During dealloying, conversely, the response of the material changes abruptly and an absorbing state clearly manifests in the spectrum. Quite remarkably, such state is formed in an ultrathin layer ( $\approx 10$  nm) and its wavelength can be precisely adjusted in the broadband range 200–400 nm. For a thickness

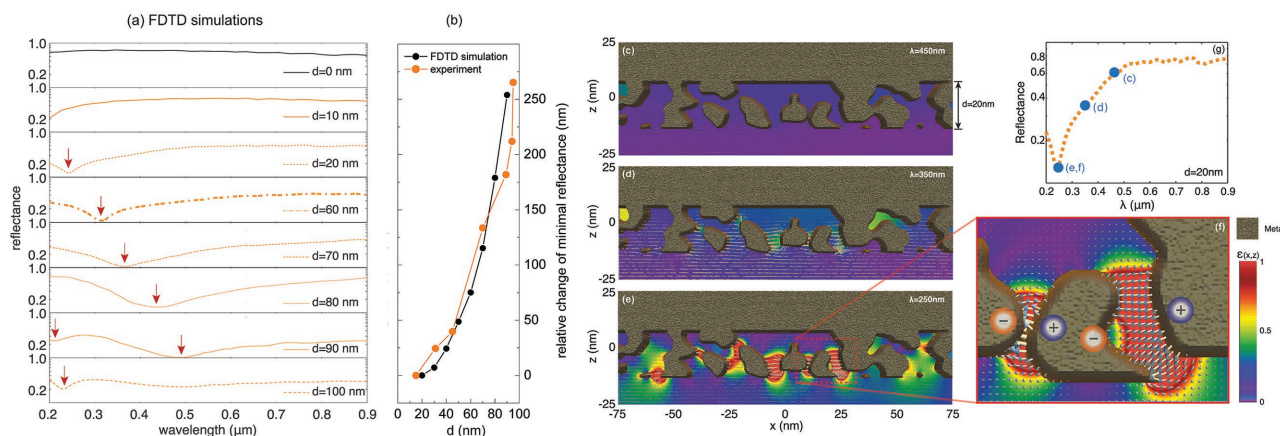


**Figure 2.** Near-normal incidence reflectance and FDTD simulations. a) Normal-incidence reflectance spectra obtained from the 2D-FDTD simulations as function of the thickness  $d$  of the disordered layer, respectively. The minima of the reflectance spectra are indicated by red arrows. b) Comparison of the experimental and simulated change in minimal reflectance as function of the thickness  $d$  of the disordered layer as obtained from the experiment. Panels (c–f) show the time-dependent electromagnetic energy density  $\varepsilon(x, z) = \frac{1}{2}(\varepsilon E^2 + \mu H^2)$  (pseudocolor plot), with  $\mathbf{E}$ ,  $\mathbf{H}$  the electric and magnetic field, respectively, and the field lines (solid arrows) of the electric field  $\mathbf{E}$  in a network material characterized by a disordered metallic network with a thickness of  $d = 20$  nm. Each panel shows the system response to a monochromatic excitation at different wavelengths: c)  $\lambda = 450$  nm, d)  $\lambda = 350$  nm, and e)  $\lambda = 250$  nm. Panel (f) provides a zoomed view of the red dotted area of panel (c), where we also illustrated the regions of positive and negative charges with symbols  $\oplus$  and  $\ominus$ . The simulated reflectivity spectrum of the sample, as well as the corresponding positions of the monochromatic excitations, are reported in panel (g). The blue dots represent the reflectivity values calculated by the FDTD simulations corresponding to the excitation wavelength (450, 350, 250 nm).

of  $d = 70$  nm and  $t_d = 4$  s the reflectivity minimum drops to 0.006 and a perfect absorbing state is created.

Wavelength control is achieved by changing the dealloying time, which systematically redshifts the reflectance minimum when the thickness of the dealloyed layer  $d$  increases. This effect is reminiscent of spherical nanospheres,<sup>[42]</sup> in which the resonance quadratically redshifts as a function of their characteristic radius. For dealloyed layers with thicknesses approaching 100 nm, we observe a second absorbing state that manifests around 200 nm (Figure 1c, Figure 2a), making the dynamics even more counterintuitive.

In order to interpret these results, we first realized a series of 2D, massively parallel finite-difference time-domain (FDTD) simulations, where we built a model of metallic networks that matches the average randomness and connectivity of our system. In our simulations we do not employ any fitting parameter. We employed 2D simulations in order to reproduce the average disorder of our samples through scanning electron microscope images from FIB polished cross-sections (Figure 2c). Our model is characterized by a percolation network with isotropic Gaussian correlation function,<sup>[43]</sup> which fits our fabricated samples as measured from SEM images. More details on the FDTD simulations can be found in the Supporting Information online text. Figure 2a reports the normal incidence reflectance spectra calculated from FDTD simulations. The numerically computed spectra show a good agreement with the experiments, illustrating the tunable absorbing state observed in our experiments and its systematic redshift for increasing thickness  $d$  of the dealloyed layer along with the appearance of a second reflectance minimum. The quantitative prediction of our FDTD models agrees well with the experimental values (Figure 2b). This is a very important result, especially considering that our model reproduces the disorder of the

sample on average, while furnishing realizations that might differ from point-to-point in the sample (see the Supporting Information, Figure 3a,b). This indicates that the measured reflectivity spectra are stable and repeatable, while not relying on the specific realization of disorder—which differs from sample to sample and is never repeated—but only on its average properties.

We investigated the physical reasons behind these effects by first analyzing the resonant state. To this extent, we considered a sample characterized by  $d = 20$  nm, and calculated the energy distribution (Figure 2c–e pseudo color plot) and the electric field force lines (Figure 2c–e solid arrows) corresponding to the material response when illuminated by a monochromatic source at wavelengths, which cover different parts of the reflectivity spectrum (Figure 2g). Far from the reflectivity minimum, when the monochromatic source is set at  $\lambda = 450$  nm, the response of the system is characterized by an almost constant electromagnetic field that does not exhibit any modulation of intensity (Figure 2c,d). The situation abruptly changes when the input wavelength moves near the reflectivity minimum at  $\lambda = 250$  nm (Figure 2e,f). In this situation we observe the generation of a complex pattern of localized hot spots, with each hot spot resembling a dipole-like resonance characterized by opposite charge concentrations (see Figure 2e and the zoomed portion in Figure 2f).

The localization of energy generated in the single hot-spot in Figure 2f shows a remarkable similarity with subwavelength light confinement observed in metallic nanoparticles. These systems, thanks to a size much smaller than the skin depth,<sup>[42]</sup> are able to localize the energy into very narrow energy spots. This fundamental property might enable a number of applications in nanoplasmonics, ranging from ultrafast control of light, to nanolasing, single molecule imaging, energy harvesting and beyond.<sup>[42,44,45]</sup> Our dealloyed networks do not encompass

nanoparticles and is conversely based on a percolating metallic thin film. However, the complex nanowire network created during the dealloying process imposes a characteristic length scale that suppresses the diffusion of surface plasmon (SP) waves,<sup>[46]</sup> localizing energy in a quasi-static configuration of dipole-like charges.

Figure 2e shows that different dipole-like states mold the flow of electromagnetic energy, concentrating the electric field lines in random positions that follow the geometric connectivity of the metal (Figure 2e). The distribution of dipole-like charges observed in Figure 2c–f does not manifest long-range order and forms a structurally disordered network of hot energy spots localized at the nanoscale. The complexity of such system cannot be analyzed by effective index parameters or classical mixing rules,<sup>[47]</sup> as any homogenization approach would average out the hot-spots. These are essential for the formation of absorbing states in the system response, as illustrated by our FDTD simulations in Figure 2c–f. We therefore provide an alternative approach, which combines ideas from graphs<sup>[48]</sup> and time-dependent coupled mode

theory (TDCMT).<sup>[49]</sup> The TDCMT is a simple and powerful approach<sup>[18]</sup> that decomposes the solution of Maxwell equations into a series of resonances. The description of this approach is detailed in ref. [50]. A detailed description of this approach is provided in the Supporting Information online text, while we here summarize the main findings. Figure 3a provides a pictorial representation of the random network of dipole-like states originated when light interacts with our structure. With reference to our material, we can intuitively represent resonant states by standing wave patterns that originate from dipole-like resonances existing at different frequencies. In the network, the distribution of resonances is represented as a distribution of nodes, with each node being a dipole-like resonance, and a random series of links, with each link representing a dipole–dipole coupling between two different dipole resonances (Figure 3a). The distribution of links identifies the functional connectivity, which determines the global response of the material. In our system, the connectivity is characterized by two different aspects: (i) in the number of links departing from each resonance, and (ii) in the strength of

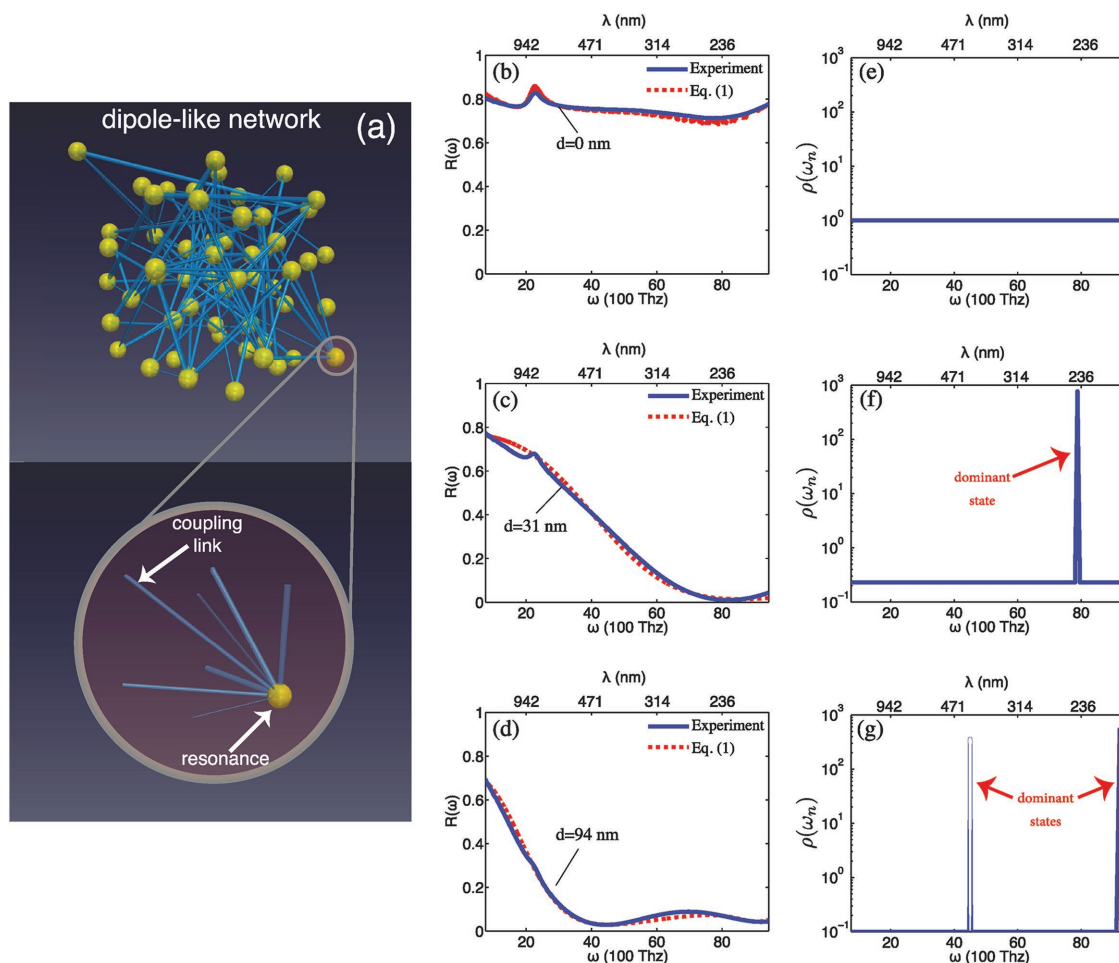


**Figure 3.** Different phases of a network material controlled by changing the connectivity of the dipole-like network. a) Schematic representation of the dipole-like network as a random network of electromagnetic dipole-like resonances, connected by random coupling links. Panels (b–d) report the experimental measured (solid blue line) and theoretically calculated (dashed red line) reflectivity spectra of fabricated samples for different dealloying times and nanowire thickness  $d$ . Panels (e–g) show the corresponding density of states  $\rho(\omega_n)$  used in the TDCMT calculations. Theoretical calculations are performed by using Equation (1) with  $N = 1000$  resonances.

each link. The number of connections per resonance describes the topology of the dipole-like network, and depends on the geometric connectivity of the nanowires, which can enable or disable connectivities according to the spatial distribution of nanowires. The strength of each link, conversely, measures the amplitude of the coupling between two dipole-like resonances and depends on the spatial overlap between the corresponding electromagnetic fields. In order to differentiate this contribution from the former, we refer to this as “electromagnetic” disorder, i.e., disorder that arises from random electromagnetic overlaps in space. The material’s response is characterized by the number of connections found in each resonance and the corresponding electromagnetic disorder. Within this representation, the reflectivity  $R(\omega)$  of the material is found to be (Supporting Information online text)

$$R = \sum_n \frac{R_n}{N} = \frac{1}{N} \sum_n \frac{(\Gamma_{cn} - \alpha_n)^2 + (\omega - \omega_n)^2}{(\Gamma_{cn} + \alpha_n)^2 + (\omega - \omega_n)^2} \quad (1)$$

where  $\omega_n$ ,  $\Gamma_{cn}$ , and  $\alpha_n$  are the oscillation frequency, outcoupling, and absorption loss, respectively, of the  $n = 1, \dots, N$  spectral eigenstates of the random network. The latter describe the dynamics of the dipole-like in terms of a new set of noninteracting modes. Details on the expressions of the various terms  $\omega_n$ ,  $\Gamma_{cn}$ , and  $\alpha_n$  appearing in Equation (1), as well as the calculation of the modes of the network, are found in the Supporting Information online text. Theoretical analysis shows that the dipole-like network possesses two different phases, which can be triggered by a variation in the network connectivity (see the Supporting Information). In the regime of strong connectivity, the features of electromagnetic disorder are completely smeared out and the system response is that of a broad-band metallic reflector (see Supporting Information, Figure S5a). Conversely, when the network connectivity is reduced to  $\approx 2$ , the features of electromagnetic disorder emerge, triggering the formation of absorbing states in the system response (see Supporting Information, Figure S5b). As shown in the Supporting Information, each absorbing state originates from a scale of electromagnetic disorder, which creates macroscopically dominant states in the resonance spectrum, inducing a destructive interference effect and the formation of a reflectivity minimum.

We validate our theory against experimental results by analyzing the experimental spectra of Figure 2a with Equation (1). As a standard approach in the TDCMT, we used the distribution of resonance function  $\rho(\omega_n)$  as a fitting parameter. Figure 3b–d reports the calculated TDCMT (dashed red line) and experimentally measured (solid blue line) reflectivity spectra, while Figure 3e–g shows the corresponding density of states used in the theoretical calculations. In the undealloyed case (Figure 3b,e), the dense metallic film shows a high reflecting response, which is very well represented by our TDCMT approach by a network of fully connected resonances with a flat density of states (Figure 3e). This originates from the fact that in a metallic structure with no pore structures, surface electric charges are free to move in every direction and show the maximum connectivity possible. The small peak at wavelength of 850 nm in Figure 3b is assigned to interband transitions due to the presence of Al in the film, a well-known

feature of aluminum.<sup>[51]</sup> In the presence of metallic nanowires (Figure 3c,d), conversely, the network connectivity becomes reduced, triggering the generation of a different material response. We calculated the mean nanowire connectivity by counting the number of touching nanowires per junction from the SEM images of the samples (see the Supporting Information online text). For  $d \in [10 \text{ nm}, 270 \text{ nm}]$ , we obtained a mean connectivity in the range  $\in [1.5, 2.6]$ . In such a reduced connectivity regime, and in good agreement with our theory, the material shows the formation of macroscopically dominant states in the resonance spectrum (Figure 3c,d,f,g). In the case of  $d = 31 \text{ nm}$ , we observe the clear appearance of a single macroscopically dominant state (Figure 3f), which originates an electromagnetic absorbing state at  $\approx 230 \text{ nm}$  (Figure 3c). For a larger nanowire network, randomness grows stronger and for  $d = 94 \text{ nm}$  we observe the emergence of a secondary scale of disorder (Figure 3d,g), which induces the formation of a second absorbing state lying in the ultraviolet (Figure 3d).

We have derived and experimentally confirmed a generalized approach to design and fabricate a new class of network metamaterials. These structures do not rely on the concept of identical building blocks. Similar to complex systems, our materials are based on the connectivity among a large number of fully heterogeneous units, which are arranged in random networks. Despite the lack of both symmetry and long-range order, these systems possess complex light–matter interactions, which we here observed in the formation of controllable absorbing states, tunable in a large optical window and originating in ultrathin material regions. We demonstrate that the absorbing states result from random hot spots in the metallic network. This form of light localization goes beyond the classical limit of effective parameters, which are usually employed to characterize metamaterials. A combination of analytical and numerical techniques explained these dynamics by introducing the concept of a dipole-like network, which characterizes the distribution of charges at the metal–dielectric interface of the complex metastructure. The functional connectivity of different dipole-like resonances leads to different phases in the material response, which can be continuously adjusted from a reflector to a perfect absorber.

The random nanowire networks introduced in this work open up new possibilities, both in metamaterial research and in material science. One of the most challenging issues that hampers the large scale exploitation of metamaterials, at optical wavelengths, lies in the fabrication of the samples. According to the recent review,<sup>[7]</sup> none of the existing techniques would allow the production of identical 3D nanostructures beyond the gram level. The nanowire networks used in this work are fabricated by simple wet-chemistry and are not constrained with respect to their active area. In addition, our Pt-Y-Al films can sustain very high temperatures,<sup>[30]</sup> making them a quite promising candidate for high temperature applications in energy harvesting, such as thermovoltaics. These applications are naturally enabled by the presence of an absorbing state.<sup>[52]</sup> By engineering random metallic networks with repeatable techniques, such as the one illustrated in this work, we can generate highly absorbing states on demand, irrespective on the microscopic details of the sample but relying only on its average connectivity.

## Supporting Information

Supporting Information is available from the Wiley Online Library or from the author.

## Acknowledgements

H.G. and A.F. contributed equally to this work. H.G. designed and performed the experimental research and fabricated and analyzed the samples used in the article. A.F. designed the theoretical research, developed the network approach based on functional connectivity, and performed FDTD simulations. M.D. performed the Rutherford backscattering experiments. F.C. suggested experiments and contributed to the interpretation. All authors contributed equally to the preparation of the manuscript. H. Galinski gratefully acknowledges financial support from the Size Matters! project, (TDA Capital, UK). Sincere thanks are given to the EMEZ (Electron Microscopy Center, ETH Zurich) and the FIRST clean-room team for their support. A. Fratolocchi and F. Capasso acknowledge funding from KAUST (Award No. CRG-1-2012-FRA-005). F. Capasso and H. Galinski acknowledge the support of Air Force Office of Scientific Research (MURI: FA9550-14-1-0389). The authors declare that they have no competing financial interests. H. Galinski thanks M. Fiebig and M. Lilienblum from the Laboratory for Multifunctional Ferroic Materials (ETH Zurich) for access to the micro-spectrophotometer. A. Fratolocchi thanks P. Magistretti for fruitful discussions about brain functions and neural networks. This work was performed in part at the Center of Nanoscale Systems (CNS), a member of the National Nanotechnology Coordinated Infrastructure Network (NNCI), which is supported by the National Science Foundation under NSF award no. 1541959. CNS is part of Harvard University.

Received: July 20, 2016

Revised: October 10, 2016

Published online: December 27, 2016

- [1] N. Engheta, *Science* **2007**, *317*, 1698.
- [2] A. Silva, F. Monticone, G. Castaldi, V. Galdi, A. Alú, N. Engheta, *Science* **2014**, *343*, 160.
- [3] N. Yu, F. Capasso, *Nat. Mater.* **2014**, *13*, 139.
- [4] N. Yu, P. Genevet, M. A. Kats, F. Aieta, J.-P. Tetienne, F. Capasso, Z. Gaburro, *Science* **2011**, *334*, 333.
- [5] E. Prodan, C. Radloff, N. J. Halas, P. Nordlander, *Science* **2003**, *302*, 419.
- [6] B. Luk'yanchuk, N. I. Zheludev, S. A. Maier, N. J. Halas, P. Nordlander, H. Giessen, C. T. Chong, *Nat. Mater.* **2010**, *9*, 707.
- [7] C. M. Soukoulis, M. Wegener, *Nat. Photonics* **2011**, *5*, 523.
- [8] R. Maas, J. Parsons, N. Engheta, A. Polman, *Nat. Photonics* **2013**, *7*, 907.
- [9] A. Fratolocchi, C. M. Dodson, R. Zia, P. Genevet, E. Verhagen, H. Altug, V. J. Sorger, *Nat. Nanotechnol.* **2015**, *10*, 11.
- [10] C. M. Soukoulis, M. Wegener, *Science* **2010**, *330*, 1633.
- [11] C. M. Soukoulis, M. Wegener, *Nat. Photonics* **2011**, *5*, 523.
- [12] R. Pastor-Satorras, A. Vázquez, A. Vespignani, *Phys. Rev. Lett.* **2001**, *87*, 258701.
- [13] A. Barrat, M. Barthélemy, R. Pastor-Satorras, A. Vespignani, *Proc. Natl. Acad. Sci. USA* **2004**, *101*, 3747.
- [14] R. Albert, H. Jeong, A.-L. Barabási, *Nature* **2000**, *406*, 378.
- [15] B. Redding, M. A. Choma, H. Cao, *Nat. Photonics* **2012**, *6*, 355.
- [16] R. Sarma, A. Yamilov, P. Neupane, H. Cao, *Phys. Rev. B* **2015**, *92*, 180203.
- [17] Y. Luo, A. Aubry, J. B. Pendry, *Phys. Rev. B* **2011**, *83*, 155422.
- [18] C. Liu, A. D. Falco, D. Molinari, Y. Khan, B. S. Ooi, T. F. Krauss, A. Fratolocchi, *Nat. Photonics* **2013**, *7*, 473.
- [19] C. Conti, A. Fratolocchi, *Nat. Phys.* **2008**, *4*, 794.
- [20] M. A. Kats, D. Sharma, J. Lin, P. Genevet, R. Blanchard, Z. Yang, M. M. Qazilbash, D. N. Basov, S. Ramanathan, F. Capasso, *Appl. Phys. Lett.* **2012**, *101*, 22, 221101.
- [21] J. D. Forster, H. Noh, S. F. Liew, V. Saranathan, C. F. Schreck, L. Yang, J.-G. Park, R. O. Prum, S. G. J. Mochrie, C. S. O'Hern, H. Cao, E. R. Dufresne, *Adv. Mater.* **2010**, *22*, 2939.
- [22] T. J. Antosiewicz, S. P. Apell, M. Zäch, I. Zoric, C. Langhammer, *Phys. Rev. Lett.* **2012**, *109*, 247401.
- [23] R. Verre, T. J. Antosiewicz, M. Svedendahl, K. Lodewijks, T. Shegai, M. Käll, *ACS Nano*, **2014**, *8*, 9286.
- [24] M. I. Stockman, *Phys. Rev. Lett.* **1997**, *79*, 4562.
- [25] V. M. Shalaev, *Nonlinear Optics of Random Media: Fractal Composites and Metal-Dielectric Films*, Springer, Berlin, Germany **2013**.
- [26] S. Gentilini, A. Fratolocchi, L. Angelani, G. Ruocco, C. Conti, *Opt. Lett.* **2009**, *34*, 130.
- [27] V. M. Shalaev, A. K. Sarychev, *Phys. Rev. B* **1998**, *57*, 13265.
- [28] C. Liu, R. E. C. van der Wel, N. Rotenberg, L. Kuipers, T. F. Krauss, A. Di Falco, A. Fratolocchi, *Nat. Phys.* **2015**, *11*, 358.
- [29] H. Galinski, T. Ryll, L. Schlagenhauf, F. Rechberger, S. Ying, L. J. Gauckler, F. C. F. Mornaghini, Y. Ries, R. Spolenak, M. Döbeli, *Phys. Rev. Lett.* **2011**, *107*, 225503.
- [30] H. Galinski, T. Ryll, Y. Lin, B. Scherrer, A. Evans, L. J. Gauckler, M. Döbeli, *Phys. Rev. Appl.* **2014**, *2*, 054015.
- [31] T. Ryll, H. Galinski, L. Schlagenhauf, F. Rechberger, S. Ying, L. J. Gauckler, F. C. F. Mornaghini, Y. Ries, R. Spolenak, M. Döbeli, *Phys. Rev. B* **2011**, *84*, 184111.
- [32] S. Supansomboon, A. Porkovich, A. Dowd, M. D. Arnold, M. B. Cortie, *ACS Appl. Mater. Interfaces* **2014**, *6*, 9411.
- [33] A.-A. E. Mel, F. Boukli-Hacene, L. Molina-Luna, N. Bouts, A. Chauvin, D. Thiry, E. Gautron, N. Gautier, P.-Y. Tessier, *ACS Appl. Mater. Interfaces* **2015**, *7*, 2310.
- [34] Z. Qi, U. Vainio, A. Kornowski, M. Ritter, H. Weller, H. Jin, J. Weissmüller, *Adv. Funct. Mater.* **2015**, *25*, 2530.
- [35] J. Biener, G. W. Nyce, A. M. Hodge, M. M. Biener, A. V. Hamza, S. A. Maier, *Adv. Mater.* **2008**, *20*, 1211.
- [36] X. Li, Q. Chen, I. McCue, J. Snyder, P. Crozier, J. Erlebacher, K. Sieradzki, *Nano Lett.* **2014**, *14*, 2569.
- [37] Q. Yun, Y.-B. He, W. Lv, Y. Zhao, B. Li, F. Kang, Q.-H. Yang, *Adv. Mater.* **2016**, *28*, 6932.
- [38] M. Raney, US 1628190 A, **1927**.
- [39] R. Liu, J. Gruber, D. Bhattacharyya, G. J. Tucker, A. Antoniou, *Acta Mater.* **2016**, *103*, 624.
- [40] R. Kraehnert, E. Ortel, B. Paul, B. Eckhardt, M. Kanis, R. Liu, A. Antoniou, *Catal. Sci. Technol.* **2015**, *5*, 206.
- [41] M. N. Y. Wang, *Handbook of Modern Ion Beam Materials Analysis*, Materials Research Society, Pittsburgh, PA, USA **2009**.
- [42] *Plasmonics: Theory and Applications* (Eds: T. V. Shahbazyan, M. I. Stockman), Springer, London, UK **2013**.
- [43] N. Garcia, E. Stoll, *Phys. Rev. Lett.* **1984**, *52*, 1798.
- [44] X. Ni, N. K. Emani, A. V. Kildishev, A. Boltasseva, V. M. Shalaev, *Science* **2012**, *335*, 427.
- [45] H. A. Atwater, A. Polman, *Nat. Mater.* **2010**, *9*, 205.
- [46] H. Raether, *Surface Plasmons on Smooth and Rough Surfaces and on Gratings*, Springer, Berlin, Germany **2013**.
- [47] P. Mallet, C. A. Guérin, A. Sentenac, *Phys. Rev. B* **2005**, *72*, 014205.
- [48] B. Bollobás, *Random Graphs*, Cambridge University Press, New York **2001**.
- [49] H. A. Haus, *Waves and Fields in Optoelectronics*, Prentice-Hall, Englewood Cliffs, NJ, USA **1984**.
- [50] J. D. Joannopoulos, S. G. Johnson, J. N. Winn, R. D. Meade, *Photonic Crystals: Molding the Flow of Light*, Princeton University Press, Princeton, NJ, USA **2008**.
- [51] H. Ehrenreich, H. R. Philipp, B. Segall, *Phys. Rev.* **1963**, *132*, 1918.
- [52] D. G. Baranov, J. H. Edgar, T. Hoffman, N. Bassim, J. D. Caldwell, *Phys. Rev. B* **2015**, *92*, 201405.